Setälä, Olli E.; Pasanen, Toni P.; Ott, Jennifer; Krainukovs, Igors; Heinonen, Juha; Vähänissi, Ville; Savin, Hele

# Elimination of dead layer in silicon particle detectors via induced electric field based charge collection

*Published in:*
Nuclear Instruments and Methods in Physics Research, Section A: Accelerators, Spectrometers, Detectors and Associated Equipment

*DOI:*
10.1016/j.nima.2024.170064

Published: 01/01/2025

*Document Version*
Publisher's PDF, also known as Version of record

Nuclear Instruments and Methods in Physics Research A 1070 (2025) 170064

Contents lists available at ScienceDirect

Nuclear Inst. and Methods in Physics Research, A

journal homepage: www.elsevier.com/locate/nima

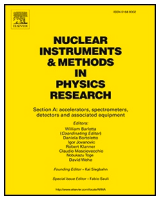

Full Length Article

# Elimination of dead layer in silicon particle detectors via induced electric field based charge collection

Olli E. Setälä [a,*], Toni P. Pasanen [a], Jennifer Ott [a], Igors Krainukovs [b], Juha Heinonen [a], Ville Vähänissi [a], Hele Savin [a]

[a] Department of Electronics and Nanoengineering, Aalto University, Tietotie 3, FI-02150, Espoo, Finland
[b] Baltic Scientific Instruments, Ramulu Str. 3, Riga, LV 1005, Latvia

ARTICLE INFO

*Keywords:*
Silicon particle detector
Dead layer
Alpha spectroscopy

ABSTRACT

The front surface of semiconductor particle detectors typically contains undepleted recombination active regions that the impinging particles pass through before reaching the sensitive area of the device. These so-called dead layers pose a fundamental limitation for achievable energy resolutions and are unavoidable in externally doped pn-junction detectors. Here, we fabricate a silicon particle detector using an alternative method for charge collection that extends the sensitive region to the front surface of the device and minimizes the dead layer. The junction is realized by inducing an electric field at the surface of the detector using a charged thin film. Such an approach has previously been implemented in photodiodes, which have demonstrated effective collection of charge carriers from the very surface of the devices. Our detector displays low leakage currents and recombination, which allow efficient charge collection throughout the device, as demonstrated by excellent internal quantum efficiency of the device. The detector is further characterized using detection of alpha particles as a case example. We achieve 20 keV energy resolutions that are, already without extensive device optimization, on the same level with commercial externally doped silicon particle detectors. Notably, the design shows promise for detection of shallow penetrating charged particles, which is very sensitive to dead layers.

## 1. Introduction

Detection of charged particles, such as alpha or beta particles and heavy ions, plays an essential role in various applications, including particle accelerators, medical imaging and safety of nuclear installations [1–6]. Semiconductor-based particle detectors have remained the most common choice for such purposes due to their high energy resolution and speed as well as small detector dimensions [7]. Of the different semiconductor materials, silicon is the most widespread choice because of its price, adaptability and extensively refined processing techniques. Other materials such as SiC, GaN, Ge, diamond, CdZnTe and CdTe have also shown promise in specific applications and operating conditions but cannot compete with the versatility of silicon [8–13].

In certain applications, mere detection of the particles is not enough. Identifying the exact energies of the detected particles is often required since it provides crucial information of their source. Within the detector, a charged particle transfers its kinetic energy to the electrons of the absorber material (here Si) resulting in a current with a magnitude proportional to the particle energy. In order to measure the energy of the particle accurately, i.e., achieve low energy resolution, all the charge carriers created by the particle must be collected. Thus, the sensitive region of the detector should cover the whole trajectory of the particle. A typical silicon particle detector design comprises a PIN structure with a high-purity n-type base and a p+ implanted layer on the front [14]. The high dopant atom concentration in the p+ region makes extending the depletion region to the surface of the detector difficult while also causing substantial Auger recombination of charge carriers generated within the doped layer [15,16]. This creates non-sensitive region, or so-called dead layer, at the front surface of the detector within which some of the particle energy is lost before reaching the sensitive depletion region of the device. The loss of energy in the dead layer causes energy straggling of the detected particles and consequently poorer energy resolution of the detector [17]. The extent of the energy straggling is proportional to the effective dead layer thickness. A common method to minimize the dead layer thickness has been to utilize a shallow p+ layer that permits thinner undepleted regions at the detector surface [15,18].

* Corresponding author.
*E-mail address:* olli.setala@aalto.fi (O.E. Setälä).

https://doi.org/10.1016/j.nima.2024.170064
Received 6 September 2024; Received in revised form 21 October 2024; Accepted 5 November 2024
Available online 10 November 2024

However, complete elimination of the dead layer is extremely challenging in a device with an externally doped junction. The dopant atoms in the implanted layer are also linked to carrier generation and hence increase the leakage current [19]. Additionally, other non-sensitive parts of the detector, such as the thin films deposited on top of its surface, can result in loss of particle energy and thus act as dead layers.

An alternative method to achieve efficient charge collection without the need for external doping atoms is to utilize an electric field induced by highly charged thin films [20]. A charged film on top of silicon creates an electric field at the silicon surface with its maximum at the thin film/Si interface. This field can, similarly to pn-junctions, separate electron-hole pairs. The most important distinction to the pn-junction is the natural extension of the electric field to the very surface of the silicon. Such induced electric fields have so far been successfully implemented at least in photodiodes as replacement for the externally doped junctions [20–22]. The absence of dopant atoms and demonstrated excellent collection efficiency all the way to the very surface of the detector indicate that these devices have no dead layer caused by the front junction. Given that there is no apparent reason why the approach would not also work for particle detectors, the induced electric field could allow reaching ultimate energy resolutions through a device with a minimal dead layer. The technology could also allow omission of the front surface doping step, hence simplifying the fabrication process and reducing the costs. Traditionally, the induced electric field has been formed with a positively charged $SiO_2$ film [20,23], but lately, negatively charged $Al_2O_3$ has emerged as an excellent alternative [21,22]. One of the main benefits of the $Al_2O_3$ for particle detectors would be its considerably better resistance to radiation-induced chargingcompared to $SiO_2$ [24,25]. $Al_2O_3$ can also provide better passivation of the Si surface than $SiO_2$ due to its strong field-effect passivation [26,27].

In this paper, we demonstrate that an efficient Si particle detector can be realized utilizing the electric field induced by an $Al_2O_3$ film for charge collection. We design and fabricate such a detector and investigate its I–V and C–V characteristics. We examine its charge collection capability and recombination activity through internal quantum efficiency (IQE), minority charge carrier lifetime and dark saturation current density ($J_0$). Furthermore, we characterize the performance of the device using the detection of 5.5 MeV alpha particles as a case example. We measure the energy spectra of a known alpha emitter and use it to determine the energy resolution of the detector. Finally, we discuss the applicability of the device in detection of other charged particles in addition to alpha particles.

## 2. Methods

The detectors in this work were fabricated on a 4-inch single side polished n-type float zone Si wafer with 350 μm thickness, ~15 kΩ cm resistivity and (111) crystal orientation. Fig. 1a shows a top view of a finished detector chip while Fig. 1b illustrates the cross-section of the device. The diameter of the circular active area is 24 mm and the width of the anode contact placed immediately outside the active area is 1 mm. The design includes 4 floating guard rings outside the anode contact for mitigation of surface leakage current emerging outside the active area.

The processing started by growing thermal $SiO_2$, which was used as an implantation mask, on the front side of the wafer. Standard photolithography was employed to pattern the $SiO_2$ followed by an ion implantation for ohmic contact formation. Front and rear sides of the wafer were implanted with boron ($1 \times 10^{15}$ $cm^{-2}$ dose and 33 keV energy) and phosphorous ($2 \times 10^{15}$ $cm^{-2}$ dose and 50 keV energy), respectively. The implantation mask was removed and a drive-in oxidation performed in an oxygen atmosphere at 1000 °C for 90 min resulting in an 85 nm thick $SiO_2$ film. The grown $SiO_2$ was patterned to open the active area and a 50 nm $Al_2O_3$ film was deposited on it with thermal atomic layer deposition (ALD) at 200 °C with water and trimethylaluminum as precursors. Due to the high negative charge (charge surface density ~$10^{12}$ $cm^{-2}$ [28]) of the ALD $Al_2O_3$ film, an electric field naturally forms under it, as shown in Fig. 1b. The direction of the electric field, and consequently movement of charge carriers, is analogous to regular pn junction detectors. Aluminum was sputtered on the front and rear sides of the wafer with thicknesses of 300 and 1000 nm, respectively. The wafer was annealed in a forming gas ambient at 425 °C for 30 min, which simultaneously served as the sintering of Al contacts and the activation of the passivating effect of $Al_2O_3$. Finally, the front side Al was patterned to form the contacts and guard rings.

The critical detector parameters were characterized from the finished devices. First, the dark I–V characteristics of the devices were measured using a Hewlett-Packard Model 4145A Semiconductor Parameter Analyzer. The C–V characteristics were then determined using 100 kHz measurement frequency with a Hewlett-Packard Model 4192A LF Impedance Analyzer. A BT Imaging LIS-R2+ was used for lifetime calibrated photoluminescence imaging (PLI) of the samples as described in Ref. [19]. Dark saturation current density ($J_0$) was obtained with a quasi-steady-state photoconductance (QSSPC) method using a Sinton Instruments WCT-120TS. $J_0$ was measured from a symmetrical test sample with two-sided $Al_2O_3$ coating and no implantations and thus only describes the recombination mechanisms present in the active area. The PL image and $J_0$ both provide information about the recombination properties of the front surface.

The ability of the detector to collect charge carriers created at different depths beneath its surface was investigated by measuring its IQE with different wavelengths of light. IQE represents the percentage of charge carriers created by light that are collected before undergoing recombination. Since different wavelengths are on average absorbed at varying distances from the surface, IQE can provide an estimation of how efficiently the device collects charge carriers created at different depths. Light was used, instead of charged particles, to create the charge carriers due to the simplicity of the measurement and controllability of the charge creation depth. To obtain the IQE, we needed to first measure the external quantum efficiency (EQE) and total spectral reflectance (R) of the detectors. EQE describes the ratio of collected charge carriers to incident photons, quite similarly to IQE, except that it also takes the optical losses into account and thus is not directly a relevant parameter regarding the detection of charged particles. Since the optical losses at wavelengths shorter than 1000 nm mainly consist of the reflectance of

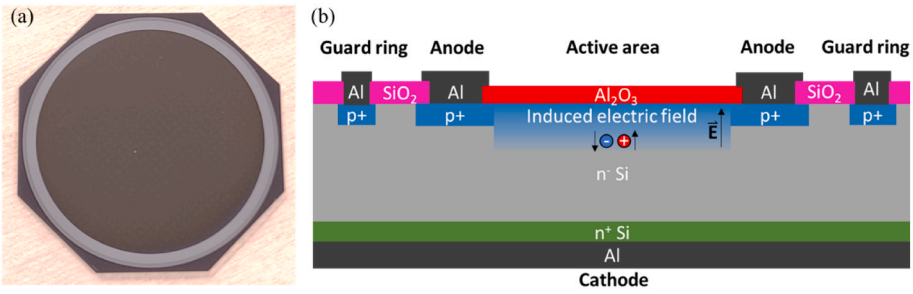


**Fig. 1.** (a) A photograph of our particle detector. (b) A schematic cross-section of the device. Only the innermost guard ring is shown in the illustration.

the surface (ALD $Al_2O_3$ is transparent to light), IQE can be calculated with $IQE = \frac{EQE}{(1-R)}$. However, the equation is inaccurate at longer wavelengths due to transmission of light through the wafer. The EQE of the devices was measured using a quantum efficiency measurement system QEX10. In the measurement, the detector was placed in a dark box and illuminated with selected wavelengths between 360 and 1070 nm (with 10 nm intervals) using a xenon arc light source and a monochromator. The light beam was focused perpendicularly on the active area of the detector and the light-generated current was measured from the terminals of the device. The current was converted to EQE by calibrating the values against a photodiode that had been calibrated using standards traceable to the National Institute of Standards and Technology (NIST). R of the detector was obtained using a UV–vis–NIR Agilent Cary 5000. The detector was placed inside an integrating sphere and illuminated with wavelengths between 360 and 1070 nm. Light reflected from the detector surface was collected by the integrating sphere and quantified by a photodetector to determine the portion of reflected light. For reference, our detector exhibited R of 11–41% and EQE of 50–88% over the observed spectrum. For the shortest wavelength (360 nm), which is the most interesting for this study due to its shallow penetration depth, the values were 23% and 78%, respectively. IQE was calculated from EQE and R and the illumination wavelengths were converted to their respective $1/e$ absorption depths (i.e., penetration depths) in silicon, providing an estimation of the IQE at different depths. Since the penetration depths vary vastly across the measured wavelength range, the test provides meaningful information about different parts of the detector.

Finally, pulse height spectra measurements were conducted at Baltic Scientific Instruments (BSI) using $^{238}Pu$ as an alpha particle source. The measurements were repeated applying reverse biases from 5 to 70 V and the obtained pulse height spectra were converted to energy spectra. The energy resolution of the detectors was determined from the full width at half maximum (FWHM) of the highest measured energy peak.

## 3. Results and discussion

Fig. 2a presents the capacitance of the particle detector fabricated in this work as a function of the reverse bias voltage. The capacitance behaves similarly to a doped junction photodiode, decreasing as the width of the depletion region increases and finally saturating to ~29 pF/cm$^2$. The saturation capacitance also corresponds well to a parallel plate capacitance value calculated with the detector dimensions, 29.6 pF/cm$^2$, confirming that the depletion region forms beneath the whole active area and not for example only under the contact ring doping. The reverse bias required for extending the depletion region all the way through the detector (i.e., the depletion voltage) can be attained from $1/C^2$ plot as shown in the inset of Fig. 2a. Full depletion is reached at 25 V reverse bias.

The dark I–V characteristics of a reverse biased detector are shown in Fig. 2b. At full depletion, the leakage current density is 4 nA/cm$^2$, which is comparable to commercial externally doped silicon detectors. Maintaining a low level of leakage current is important to mitigate noise and preserve the energy resolution. In our design, we have incorporated multiple guard rings surrounding the anode to minimize the influence of surface leakage. The absence of dopant atoms, which are known for acting as generation centers, should also limit the leakage current in our device. Considering these design factors, the leakage current is surprisingly high. In fact, photodiodes utilizing similar induced electric field structure have achieved <1 nA/cm$^2$ leakage current [29], and there is no reason why similar values would not be possible with particle detectors too.

The inset in Fig. 2b shows a lifetime calibrated PL image of the detector that demonstrates the exceptional electrical quality of the $Al_2O_3$-coated active area. It exhibits ~2000 μs minority carrier lifetime, while, for example, the surrounding $SiO_2$ areas maintain a level of ~400 μs. High carrier lifetime indicates that the $Al_2O_3$ thin film can effectively mitigate surface recombination. Combining the low surface recombination with the naturally induced electric field and a high-quality bulk material makes efficient collection of charge carriers possible. Since charge carrier recombination and generation are linked processes, minimizing the recombination can also decrease the leakage current [19]. Finally, the dark saturation current density ($J_0$) of the device is determined. $J_0$ describes the collective sum of the recombination mechanisms that take place at the surface of the device and within the depletion region, hence providing a convenient way to compare different devices. $J_0$ of our detector is 2.4 fA/cm$^2$, which is on the same level with earlier induced electric field devices (3 fA/cm$^2$) that exhibit extremely low recombination [30,31]. Excellent $J_0$ value further demonstrates the capability of our detector to efficiently collect charge carriers.

Next, a direct investigation of the internal charge collection efficiency of our detector is performed by illuminating the device with different wavelengths of light and calculating the corresponding IQE. Fig. 3 exhibits the zero bias IQE as a function of the penetration depth of different wavelengths of light. The experiment emulates charge creation at different depths and provides information about the device performance near the surface and deeper in the bulk. The device collects virtually all charge carriers created within the first 100 μm of the detector. Most impressively, charges created within a mere 10 nm from the surface are collected with 100% efficiency. It must be noted, that due to the impact ionization phenomenon, high energy photons can create more than one electron-hole pair at wavelengths <400 nm [32], which is seen as IQE>100%. Therefore, in this region, IQE can slightly

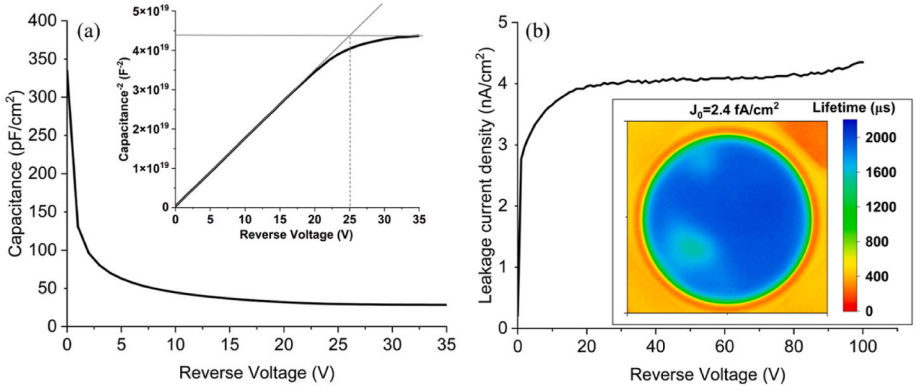


**Fig. 2.** (a) The capacitance of our particle detector at varying reverse bias voltages. Inset: $1/C^2$ curve with grey lines depicting extensions for linear and saturation regions and their intersection indicating the depletion voltage. (b) The leakage current density of the device at varying reverse bias voltages. Inset: Lifetime calibrated PL-image of the device with $J_0$ value presented.

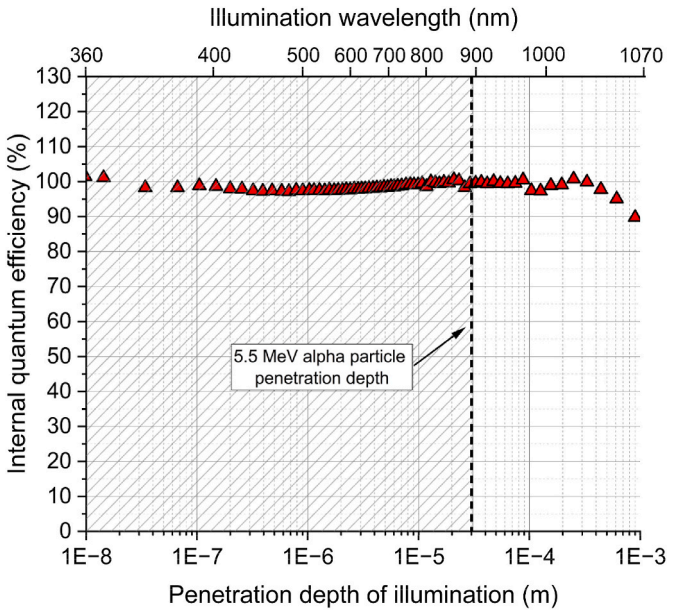


**Fig. 3.** The IQE of our detector as a function of the penetration depth of illumination. The top vertical axis depicts the wavelengths of light that correspond to the penetration depths.

overestimate the corresponding charge collection efficiency at that certain depth. Nevertheless, with the wavelengths employed in this work the effect of impact ionization is not substantial. The results showcase the absence of junction-originated dead layer along with the otherwise excellent performance of the detector. Vertically uniform collection efficiency also makes the device less sensitive to variations in the incident angles of the impinging particles. Since the charge carriers are collected similarly from all parts of the detector, the propagation path of the particles should not impact the amount of collected charge. This allows accurate operation also at close detector-source spacing at which the particles can enter the detector at various angles.

Although the excellent charge collection indicates the absence of dead layer within the silicon surface, the $Al_2O_3$ thin film on top of it acts as one itself. Since light, unlike charged particles, can pass freely through the $Al_2O_3$ layer, the dead layer created by the film is not visible in the results shown in Fig. 3. In reality, a charged particle would lose some of its energy while passing through the thin film. In this work, the thickness of the $Al_2O_3$ film is 50 nm. Such a dead layer thickness does not have a considerable effect on highly energetic particles with deep penetration depths but may impact particles with shallower penetration depths. Nevertheless, in order to minimize the effective dead layer thickness, it would be possible to reduce the thickness of the $Al_2O_3$ film down to 5 nm without compromising its passivation and field formation capabilities [33–35]. As mentioned in the introduction, another important issue to consider is the radiation endurance of the $Al_2O_3$ film. Although this topic is not studied in our work, relevant literature is available. It has been shown that a device utilizing $Al_2O_3$-based induced electric field charge collection similar to this work only experiences a minor degradation in the collection efficiency after proton and electron irradiation, while the passivation ability of the film remains excellent [25]. Similarly, gamma radiation has been shown to have a minimal effect on collection efficiency [36] and the passivation [24] of devices coated with ALD $Al_2O_3$. These results are mainly associated with the resilience of $Al_2O_3$ to film charging.

Finally, as a case example for charged particle detection, we employed our detector for detection of alpha particles. The most important parameter in alpha spectroscopy is the energy resolution of the detector. It determines whether the detector can resolve particles, which have energies close to each other. Although alpha particles created in specific nuclear reactions are monoenergetic, non-idealities within the detector broaden the detected energy spectrum. The primary causes for hindered energy resolution in silicon particle detectors include energy straggling in the dead layer, statistical noise, and inefficient charge collection [37]. Due to these non-idealities, simultaneously measuring two sources with nearly identical energies may result in overlapping energy spectra. For example, $^{238}$Pu decays with two alpha decay energies: 5456.3 and 5499.1 keV. In order for a detector to distinguish these two decay processes, its energy resolution must in general be smaller than the difference in the particle energies, i.e., in this case $<$42.8 keV.

Fig. 4a depicts the energy spectrum of $^{238}$Pu measured with our detector at 25 V reverse bias (depletion voltage). The energy spectrum displays two discernible peaks corresponding to the previously mentioned two different alpha decay energies. The result demonstrates that a good energy resolution can be achieved with a device utilizing a charged thin film induced electric field. More specifically, the energy resolution of the device can be defined as the FWHM of the peaks and is shown to be 20 keV in the case of 5499.1 keV alpha particles. The energy resolution of our detector is on the same level with similarly sized commercial ion implanted silicon alpha detectors (15–20 keV [38–40]) confirming it as a viable option for precision particle spectroscopy. One fundamental difference between the commercial detectors and the device reported here is the electric field at the front surface. The externally doped commercial devices require a high operating voltage to extend the electric field to the front surface, whereas our device achieves it naturally at zero bias. Therefore, the optimal performance of our particle detector could already be achieved using low operating voltages.

To further analyze the impact of the bias voltage, the pulse height spectra obtained using our device at reverse bias voltages of 5, 10, 25, and 70 V are illustrated in Fig. 4b. An energy resolution of ~20 keV can already be achieved at a bias voltage of −10 V. There is little difference in the pulse height spectra above −10 V bias demonstrating that the detector does not need to be fully depleted to operate well. However, operating the detector at or beyond full depletion not only reduces the capacitance, but also increases drift speed of carriers and minimizes the series resistance of the highly resistive intrinsic layer ($n^-$), all of which improve the speed of the device [41]. The resistance of the non-depleted region is also a significant source of noise, which appears to impact the energy resolution of the detector at lower biases. The effect is especially prominent in our device due to the high resistivity of the bulk material making operation at or beyond full depletion (>25 V) preferable. Indeed, at −5 V bias the energy resolution of our detector is poor and the spectrum is not divided. It should be noted that the depletion region extends beyond the range of the 5.5 MeV alpha particle already at −5 V bias and the impact of collection efficiency on the energy resolution should thus be minimal.

Although the energy resolution of our device could not yet surpass the commercial silicon alpha detectors, the results are promising and indicate a possibility for further improvements. Since the charge collection efficiency of the device is shown to be nearly perfect, the possible ways to improve the energy resolution would be reducing the overall device noise and the dead layer thickness caused by the surface thin film. As discussed earlier, the dead layer in our device arises solely from the 50 nm $Al_2O_3$ film, whose thickness could be reduced to 5 nm to virtually eliminate the dead layer. Nevertheless, in the case of energetic alpha particles, the impact of even 50 nm dead layer on the energy resolution is minimal. An alpha particle with 30 μm penetration depth loses roughly 0.1% of its energy within such a thin film, which is low enough to not cause substantial energy straggling. Therefore, the room for improvement in energy resolution is likely caused by device noise, i.e., leakage current, which we believe could be reduced by further process optimization.

Since the impact of thin dead layers on detection of 5.5 MeV alpha particles is marginal, the benefits of our detector should be more pronounced in the detection of particles with shallow penetration depths, e.

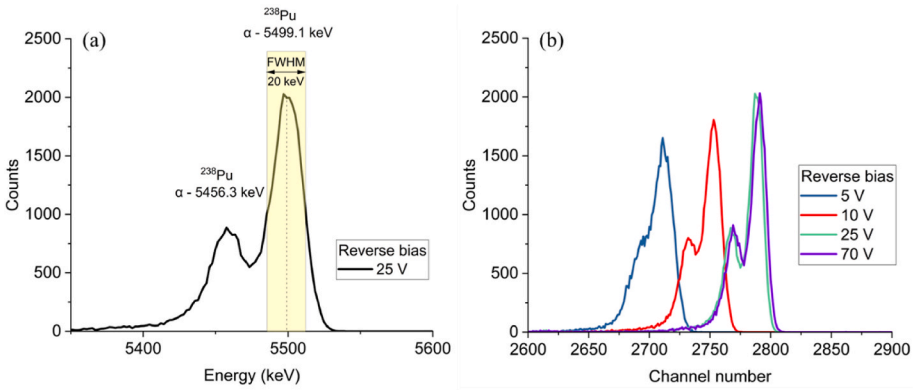


**Fig. 4.** (a) The energy spectrum of an alpha emitting $^{238}$Pu measured with our particle detector at 25 V reverse bias. Two peaks represent the two alpha decay processes of $^{238}$Pu that produce alpha particles with slightly different energies. FWHM is presented for the higher peak. (b) The pulse height spectra measured at varying reverse biases.

g., electrons or alpha particles with low energies. For such particles, the thickness of the dead layer has significantly larger effect on the energy resolution, which makes the device with reduced $Al_2O_3$ film thickness an excellent option. For example, the penetration depth of 10 keV electrons is $< 1$ μm [42]. This means that the typical dead layer thicknesses of silicon particle detectors (~50–100 nm [40,43]) account for a considerable portion of the propagation path and thus drastically hinder the energy resolution. Conversely, only a 5 nm dead layer resulting from $Al_2O_3$ would not cause major limitation for the detection.

## 4. Conclusions

Silicon particle detectors based on a charged thin film induced electric field have been manufactured and characterized. We have demonstrated that induced electric field technology, which has earlier been implemented to photodiodes, can be used for detection of highly energetic particles as well. By utilizing the induced electric field, it is possible to effectively eliminate the dead layer typically found in conventional devices with externally doped junctions. The fabricated devices demonstrate perfect charge collection throughout the entire detection volume, notably encompassing even the first 10 nm of the silicon substrate. As a result, our detector already displays energy resolution and leakage current performance comparable to commercial implanted junction counterparts, even without extensive device optimization. With further development, the induced electric field technology could provide unparalleled detection efficiency for charged particles with shallow penetration depths, as it has already demonstrated in the realm of photodetection. Furthermore, our detector can be operated with moderate reverse biases, as it reaches ~20 keV energy resolution already with −10 V bias. Finally, fabrication of an electric field inducing layer is simple as it only requires deposition of the charged film, which can simultaneously be used for surface passivation. This simplifies and reduces the cost of the detector fabrication process, as the doping phase can be omitted.

## CRediT authorship contribution statement

**Olli E. Setälä:** Writing – review & editing, Writing – original draft, Visualization, Validation, Methodology, Investigation, Formal analysis, Data curation, Conceptualization. **Toni P. Pasanen:** Writing – review & editing, Methodology, Investigation, Formal analysis. **Jennifer Ott:** Writing – review & editing, Methodology, Investigation, Formal analysis. **Igors Krainukovs:** Writing – review & editing, Methodology, Investigation. **Juha Heinonen:** Writing – review & editing, Methodology, Investigation, Formal analysis. **Ville Vähänissi:** Writing – original draft, Validation, Supervision, Resources, Project administration, Funding acquisition, Formal analysis, Conceptualization. **Hele Savin:** Writing – original draft, Validation, Supervision, Resources, Project administration, Funding acquisition, Formal analysis, Conceptualization.

## Declaration of competing interest

The authors declare that they have no known competing financial interests or personal relationships that could have appeared to influence the work reported in this paper.

## Acknowledgements

The authors acknowledge the provision of facilities and technical support by Micronova Nanofabrication Centre and Nanomicroscopy Centre in Espoo, Finland within the OtaNano research infrastructure at Aalto University. The work was funded through the ATTRACT project funded by the European Commission (EC) under Grant Agreement 777222 and by Business Finland through project RaPtor (687/31/2019). The work is related to the Flagship on Photonics Research and Innovation "PREIN" funded by the Academy of Finland.

## Data availability

The data that support the findings of this study are openly available in Zenodo at https://doi.org/10.5281/zenodo.13683410.

## References

[1] H. Vincke, C. Theis, S. Roesler, Induced radioactivity in and around high-energy particle accelerators, Radiat. Protect. Dosim. 146 (4) (2011) 434–439.
[2] G. Immè, D. Morelli, M. Aranzulla, R. Catalano, G. Mangano, Nuclear track detector characterization for alpha-particle spectroscopy, Radiat. Meas. 50 (2013) 253–257.
[3] S.M. Qaim, I. Spahn, B. Scholten, B. Neumaier, Uses of alpha particles, especially in nuclear reaction studies and medical radionuclide production, Radiochim. Acta 104 (9) (2016) 601–624.
[4] C. Parker, et al., Alpha emitter radium-223 and survival in metastatic prostate cancer, N. Engl. J. Med. 369 (3) (2013) 213–223.
[5] A.J. Crompton, K.A.A. Gamage, A. Jenkins, C.J. Taylor, Alpha particle detection using alpha-induced air radioluminescence: a review and future prospects for preliminary radiological characterisation for nuclear facilities decommissioning, Sensors 18 (4) (2018) 1015.
[6] S. Yamamoto, J. Hatazawa, Development of an alpha/beta/gamma detector for radiation monitoring, Rev. Sci. Instrum. 82 (11) (2011) 113503.
[7] P.H. Gooda, W.B. Gilboy, High resolution alpha spectroscopy with low cost photodiodes, Nucl. Instrum. Methods Phys. Res. 255 (1–2) (1987) 222–224.
[8] K.C. Mandal, S.K. Chaudhuri, F.H. Ruddy, High-resolution alpha spectrometry using 4H-SiC detectors: a review of the state-of-the-art, IEEE Trans. Nucl. Sci. 70 (5) (2023) 823–830.
[9] G. Wang, et al., GaN-based PIN alpha particle detectors, Nucl. Instrum. Methods Phys. Res. 663 (1) (2012) 10–13.

[10] N. Fourches, M. Zielińska, G. Charles, High purity germanium: from gamma-ray detection to dark matter subterranean detectors, in: B. Almayyahi (Ed.), Use of Gamma Radiation Techniques in Peaceful Applications, IntechOpen, 2019.
[11] P. Bergonzo, et al., Particle and radiation detectors based on diamond, Phys. Status Solidi 185 (1) (2001) 167–181.
[12] L. Bao, G. Zha, J. Li, W. Jie, Preparation and characterization of CdZnTe particle detectors, J. Phys. Conf. Ser. 1635 (1) (2020) 012093.
[13] T. Takahashi, S. Watanabe, Recent progress in CdTe and CdZnTe detectors, IEEE T. Nucl. Sci. 48 (4) (2001) 950–959.
[14] Hamamatsu Photonics, Si detectors for high energy particles, available at, https://www.hamamatsu.com/content/dam/hamamatsu-photonics/sites/documents/99_SALES_LIBRARY/ssd/high_energy_kspd9002e.pdf. (Accessed 4 September 2024).
[15] R. Hartmann, et al., Low energy response of silicon pn-junction detector, Nucl. Instrum. Methods Phys. Res. 377 (2–3) (1996) 191–196.
[16] M.S. Tyagi, R. Van Overstraeten, Minority carrier recombination in heavily-doped silicon, Solid State Electron. 26 (6) (1983) 577–597.
[17] B.L. Wall, et al., Dead layer on silicon p–i–n diode charged-particle detectors, Nucl. Instrum. Methods Phys. Res. 744 (2014) 73–79.
[18] J. Dobrovodský, I. Bešše', L. Hrubčín, P. Kováč, Shallow p+n junction silicon nuclear radiation detectors, Sens. Actuators A Phys. 42 (1–3) (1994) 558–561.
[19] H.M. Ayedh, et al., Fast wafer-level characterization of silicon photodetectors by photoluminescence imaging, IEEE Trans. Electron Devices 69 (5) (2022) 2449–2456.
[20] T.E. Hansen, Silicon UV-photodiodes using natural inversion layers, Phys. Scr. 18 (6) (1978) 471–475.
[21] M.A. Juntunen, et al., Near-unity quantum efficiency of broadband black silicon photodiodes with an induced junction, Nat. Photonics 10 (12) (2016) 777–781.
[22] K. Chen, et al., Excellent responsivity and low dark current obtained with metal-assisted chemical etched Si photodiode, IEEE Sens. J. 23 (7) (2023) 6750–6756.
[23] M. Sildoja, et al., Predictable quantum efficient detector: I. Photodiodes and predicted responsivity, Metrologia 50 (2013) 385–394.
[24] M.N. Getz, M. Povoli, O. Koybasi, T. Slavicek, E. Monakhov, Gamma-radiation hardness and long-term stability of ALD-Al2O3 surface passivated Si, J. Appl. Phys. 133 (15) (2023).
[25] J. Heinonen, et al., Results on radiation hardness of black silicon induced junction photodetectors from proton and electron radiation, Nucl. Instrum. Methods Phys. Res. 977 (2020) 164294.
[26] O.E. Setälä, T.P. Pasanen, J. Ott, V. Vähänissi, H. Savin, Al-neal degrades Al2O3 passivation of silicon surface, Phys. Status Solidi 218 (23) (2021).
[27] G. Dingemans, W.M.M. Kessels, Status and prospects of Al2O3-based surface passivation schemes for silicon solar cells, J. Vac. Sci. Technol. A 30 (4) (2012).
[28] D. Hiller, D. Tröger, M. Grube, D. König, T. Mikolajick, The negative fixed charge of atomic layer deposited aluminium oxide—a two-dimensional SiO2/AlOx interface effect, J. Phys. D Appl. Phys. 54 (27) (2021) 275304.
[29] T. Tsang, A. Bolotnikov, A. Haarahiltunen, J. Heinonen, Quantum efficiency of black silicon photodiodes at VUV wavelengths, Opt Express 28 (9) (2020) 13299–13309.
[30] M. Garin, et al., Black-silicon ultraviolet photodiodes achieve external quantum efficiency above 130, Phys. Rev. Lett. 125 (11) (2020) 117702.
[31] K. Chen, et al., Harnessing carrier multiplication in silicon solar cells using UV photons, IEEE Photon. Technol. Lett. 33 (24) (2021) 1415–1418.
[32] S. Kolodinski, J.H. Werner, T. Wittchen, H.J. Queisser, Quantum efficiencies exceeding unity due to impact ionization in silicon solar cells, Appl. Phys. Lett. 63 (17) (1993) 2405–2407.
[33] G. Dingemans, R. Seguin, P. Engelhart, M.C.M. Van De Sanden, W.M.M. Kessels, Silicon surface passivation by ultrathin Al2O3 films synthesized by thermal and plasma atomic layer deposition, Phys. Status Solidi Rapid Res. Lett. 4 (1–2) (2009) 10–12.
[34] A. Richter, J. Benick, M. Hermle, S.W. Glunz, Excellent silicon surface passivation with 5 Å thin ALD Al2O3 layers: influence of different thermal post-deposition treatments, Phys. Status *Solidi RRL* 5 (5–6) (2011) 202–204.
[35] N.M. Terlinden, G. Dingemans, M.C.M. van de Sanden, W.M.M. Kessels, Role of field-effect on c-Si surface passivation by ultrathin (2-20 nm) atomic layer deposited Al2O3, Appl. Phys. Lett. 96 (11) (2010) 112101.
[36] J. Ott, et al., Characterization of magnetic Czochralski silicon devices with aluminium oxide field insulator: effect of oxidant on electrical properties and radiation hardness, J. Instrum. 16 (5) (2021) P05011.
[37] Y.K. Akimov, Silicon radiation detectors (review), instrum, Exp. Tech. 50 (2007) 1–28.
[38] Baltic Scientific Instruments, Silicon ion implanted alpha particle detectors SIID, available at, https://bsi.lv/media/product_files/alpha-detectors.pdf. (Accessed 3 June 2024).
[39] AMETEK ORTEC, ULTRA and ULTRA AS – ion-implanted-silicon charged-particle detectors, available at, https://www.ortec-online.com/-/media/ametekortec/brochures/u/ultra.pdf?la=en&revision=88b06c5e-cacd-480b-bfdb-aa358ffd6fd4. (Accessed 4 September 2024).
[40] Mirion Technologies, PIPS detectors – passivated implanted planar silicon detectors, available at, https://mirionprodstorage.blob.core.windows.net/prod-20220822/cms4_mirion/files/pdf/spec-sheets/c39313_passivated_pips_super_spec_1.pdf. (Accessed 4 September 2024).
[41] Hamamatsu Photonics, Si detectors for high energy particles, available at, https://www.hamamatsu.com/content/dam/hamamatsu-photonics/sites/documents/99_SALES_LIBRARY/ssd/high_energy_kspd9002e.pdf. (Accessed 4 September 2024).
[42] O. Kurniawan, V.K.S. Ong, Investigation of range-energy relationships for low-energy electron beams in silicon and gallium nitride, Scanning 29 (6) (2007) 280–286.
[43] G.F. Knoll, Radiation Detection and Measurement, fourth ed., John Wiley & Sons, 2010, 978-0-470-13148-0.